Chemical Science & Engineering Research

Ariviyal Publishing

Research Article

DOI: 10.36686/Ariviyal.CSER.2020.02.05.024

Chem. Sci. Eng. Res., 2020, 2(5), 17-23.

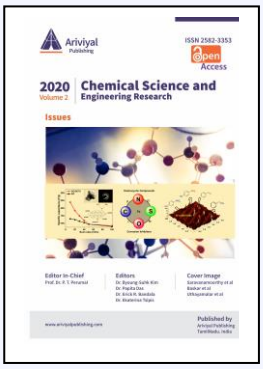

Microwave-Assisted Green Synthesis of ZnO-AlPO Composite and its Adsorption Studies

Shalini K.S.,*[a] Nirmala B*[b] and Nagaraju G[c]

[a]*Research student, Department of Chemistry, Tumkur University, Tumkur*
[b]*Assistant Professor, Department of Chemistry, Tumkur University, Tumkur, India-572102*
[c]*Energy Materials Research Laboratory, Department of Chemistry, Siddaganga Institute of Technology (Affiliated to Visvesvaraya Technological University), Tumkur – 572 103, India*

***Corresponding author E-mail address**: shalni.k.s@gmail.com (Shalini K.S); nirmala2528@gmail.com (Nirmala B)

ISSN: 2582-3353

Crossref

Publication details
Received: 05th September 2020
Revised: 08th October 2020
Accepted: 09th October 2020
Published: 27th October 2020

Abstract: Metal oxide - aluminophosphate composite was synthesized using Zinc nitrate employing the whole plant extract of Parmelia perlata, lichen using a green synthetic method.. Whole-plant extracts of Parmelia perlata was used as an oxidizing agent to oxidize metal nitrates into corresponding oxides on the surface of aluminophosphate zeolites yielding metal oxide-aluminophosphate composites. The structure and composition of the synthesized MO-AlPO composites were confirmed by XRD, FT-IR, SEM-EDAX, HR-TEM, BET, and TGA. The surface area of the ZnO-AlPO composite was found to be 21.193 m^2/g with pore volume 0.083 cm^3/g and pore diameter 12.83 nm. Synthesized ZnO-AlPO composite was evaluated for its adsorption efficiency using methylene blue as a model pollutant.

Keywords: Aluminophosphates; Zinc oxide; Composites; Green synthesis; Parmelia perlata; Adsorption; Adsorption isotherms

1. Introduction

Metal oxides and metal oxide nanocomposites are enthralling the world of researchers with their versatility and have found to be useful as sensors, batteries, super capacitors, catalysis, pharmaceuticals etc.[1,2,3,4] Nanocomposites are synthesized with different matrices such as ceramic matrix, polymer matrix or metal matrix.[5,6,7] Polymer matrix nanocomposites encompasses polymer systems such as layered silicates, biodegradable polymers like polysachcharides, poly acetic acid, polyethylene glycol, polyvinyl alcohol etc, or conducting polymers namely polyaniline, polypyrrole, polythiophene etc.[8,9] Synthesis of nanocomposites of metal oxides with polymer matrix leads to amalgamation of desirable qualities resulting in products with engineered structural, morphological, physical and chemical properties.

Aluminophosphate zeolites are a class of silica-free zeolite materials which are fascinating scientists across the world since they were first synthesized in the 1980s.[10] Many of the aluminophosphate zeolites have a similar structural framework as zeolites but there are AlPO's with a unique structural framework[11-13] Aluminophosphate zeolites are found to be more useful as adsorbents, catalysts, gas separation, energy storage devices, etc. Zeolites are aluminosilicate molecules that invariably have a negatively charged molecular framework and to stabilize the framework charge, it would incorporate alkali and alkaline earth metals into its framework. Aluminophosphate zeolites on the contrary have a neutral molecular framework. Hence it is free of associated metal ions. However, aluminophosphate zeolites can be made to incorporate metal ions into their framework by providing suitable synthetic conditions.[14,15,16,17]

One of the major drawbacks of aluminophosphate zeolites is its neutral framework and slow diffusion rate which affects the adsorption capacity or catalytic efficiency of aluminophosphate zeolites. From various literary sources, it can be learned that the inclusion of transition metal ions, cations, or metal oxides into the zeolitic framework, enhances diffusion rates thereby strongly influencing catalytic and adsorption efficiency of the host molecules.[18,19,20] Incorporation of transition metal ions or metal oxides into the aluminophosphate framework can be achieved in three ways. In the physical method, metal oxides are crushed with pre-synthesized zeolites using an agate motor, while the chemical method involves the synthesis of metal oxides into pre-synthesized zeolite framework or co-synthesis of aluminophosphates along with metal oxides by adding metal oxide precursor to the aluminophosphate precursor gel. Many groups have reported the successful synthesis of metal oxide incorporated aluminophosphate zeolites or MO-AlPO composites.[15,16,21,22]

In the present study, we have followed the green synthesis approach for the synthesis of ZnO-AlPO composites where we have used pre-synthesized aluminophosphate zeolites and zinc nitrate as the precursor for synthesizing Zinc oxide nanoparticles. The whole plant extract of Parmelia perlata was used as an oxidizing agent.

Parmelia perlata is the lichen found commonly in Western Ghats of Karnataka, India. The lichen is rich in alkaloid content. Plant extract can therefore act as a good oxidizing agent as well as fuel for the synthesis of ZnO-AlPO composites.[23-25] The synthesized ZnO-AlPO composite was confirmed by XRD and FT-IR studies, surface morphology was studied using microscopic techniques such as SEM-EDAX-TEM, surface area analysis using BET, and thermal stability using TGA-DSC. Adsorption efficiency of the ZnO-AlPO composite was evaluated using water-soluble dye methylene blue.

2. Experimental Section

2.1. Material and Methods

Parmelia perlata was washed thoroughly with tap water followed by distilled water. The lichen was dried in shade and used to prepare plant extract. 10 g of the washed and dried lichen was refluxed with 100 ml of distilled water in a 250 ml round bottom flask for 1 hour. Contents of the flask were filtered under vacuum, cooled, and stored in an airtight container. It was refrigerated for further use. 0.58 mg of the amount of Zn $(NO_3)_2.6H_2O$ was dissolved in 10 mL of Parmelia perlata extract and suspension was stirred for 30 min. 100 mg of aluminophosphate zeolite was added to the reactive gel and was aged for 1 hour. (Aluminophosphate zeolite was synthesized under microwave irradiation using alanine as a structure-directing agent[26]). The reaction mixture was then subjected to microwave irradiation for 10 min at 600 W. The product obtained was calcined at 300°C for 3 hours. ZnO-AlPO composite thus prepared characterized using various techniques such as XRD, FT-IR, SEM-EDAX, HR-TEM, and BET.

2. 2. Characterization

Structural studies were carried out using powder XRD technique using PAN analytical X'pert PRO X-RAY diffractometer with graphite monochromatized Cu K_α radiation source (λ–1.541Å) in the range of 10°–80° with a scanning rate of 2°/min. FT-IR spectra were recorded using Brucker Alpha FT-IR Spectrophotometer. Microscopic techniques such as SEM- EDAX and TEM were used to study the surface morphology of the synthesized aluminophosphate zeolites. SEM- EDAX data was obtained using JEOL–6390LA/ Oxford XMX N, with an accelerating voltage of 0.5 to 30 kV. It employs tungsten filament, magnification up to 300000. EDAX was recorded with a resolution of 136 eV, detector area of 30 mm^2 with an inbuilt elemental mapping facility. TEM images were recorded using Joel/JEM 2100, employing 200 kV accelerating voltage, LaB6 electron gun, and point resolution up to 0.23 nm and lattice resolution of 0.14 nm along with SAED. Surface area and pore analyses were performed with NOVA–1000, VERSION – 3.70, by Brunauer Emmet Teller method (B.E.T method) and de Boer t-Plot method. Thermogravimetric analysis was carried out to test the stability of the synthesized compounds under extreme temperature for a prolonged period of time. Thermogravimetric analysis (TGA) was carried out using a thermogravimetric analyzer (TG/DSC, Model STA449F3, NETZSCH Germany) with a heating rate of 5°C per minute in an air atmosphere.

2.3. Adsorption studies

Batch sorption experiments were carried out to evaluate the efficiency of the synthesized adsorbent using methylene blue as a model pollutant. 100ml of dye solution of different initial concentrations (1, 2, 3, 4, and 5 ppm) was stirred with different amount of adsorbent dosage (2, 4, 6, 8, and 10 mg). 2 ml of the reaction mixture was withdrawn at a regular time interval, centrifuged and absorbance of the centrifugate was recorded. The results obtained were analyzed to determine various parameters such as percentage adsorption, C_e (equilibrium dye concentration, ppm), q_e (equilibrium adsorption coefficient, ppm). Data obtained by batch sorption studies were also used to understand the kinetics of the adsorption process and were fitted against various isotherm models to learn the probable mechanism of adsorption.[27-30]

The percentage of adsorption was calculated using eq 1 and q_e was calculated using eq 2.

$$\% \, adsorption \, \frac{(C_o - C_t)}{C_o} \times 100 \quad (1)$$

$$q_e = \frac{(C_o - C_e)}{weight \, of \, adsorbent} \times V \quad (2)$$

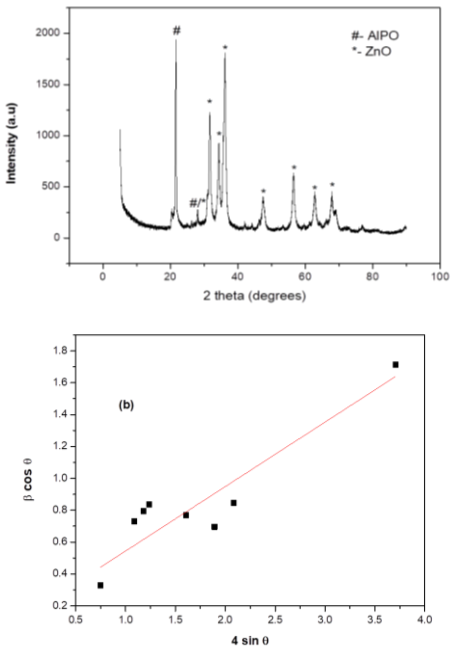

Fig. 1. (a) X-ray diffraction pattern of ZnO-AlPO composite, and (b) W-H plot of ZnO-AlPO Composite

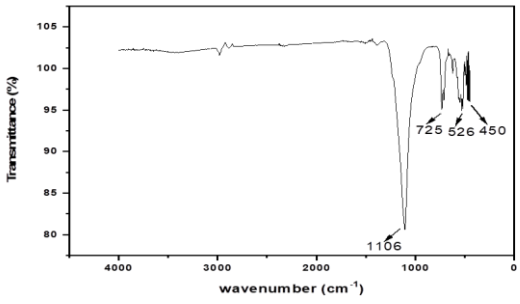

Fig. 2. FT-IR spectrum of ZnO-AlPO composite

3. Results and Discussions

3.1. X-ray diffraction studies

The XRD pattern for aluminophosphate corresponds to $AlPO_4$-tridymite (orthorhombic phase), the peaks corresponding to ZnO in the diffraction pattern of the obtained compound is compared with standard XRD patterns. Average particle size D calculated using Debye- Scherrer equation (3),

$$D = k\lambda / \beta \cos\theta \quad (3)$$

Willamson–Hall (W-H) method was used to calculate the lattice strain from the following modified Scherrer equation (4),

$$\beta\cos\theta = (k\lambda/D) + (4\varepsilon\sin\theta) \quad (4)$$

The W-H plot of βcosθ against 4sinθ is shown in Fig. 1.2. Dislocation density (δ) was estimated using equation (5).[31,32]

$$\delta = 1/D2 \quad (5)$$

XRD for ZnO-AlPO is presented in Fig. 1(a) and W-H plots are presented in Fig. 1(b). XRD plots show peaks corresponding to both AlPO and ZnO. Peaks corresponding to Aluminophosphate zeolite corresponds to the tridymite phase (orthorhombic symmetry) while peaks corresponding to ZnO in the diffraction pattern can be indexed as belonging to the pure hexagonal phase (a= 3.24982Å and c= 5.20661Å) analogous to the Zincite phase (JCPDS no- 36-1451).[26,32,33] Crystallite size, lattice strain (ε x 10^{-4}) and dislocation density (δ x1015 Lines/m^2) was found to be 39.66 nm, 0.447 and 0.63 respectively.

3.2. FT-IR studies of ZnO-AlPO composite

The Representative FT-IR spectrum of ZnO-AlPO is presented in Fig 2. It shows a strong band at 1101 cm^{-1} which corresponds to characteristic PO_4 tetrahedra. A small peak around 1100 cm^{-1} is due to Zn-OH stretching vibration. The absorption band at 734 cm^{-1} corresponds to symmetric stretching vibrations of PO_4 groups. The weak absorption peak at about 620 cm^{-1} is due to the interaction between the alumina tetrahedral of the zeolite structure and Al^{3+}. Peaks between 450 and 600 cm^{-1} correspond to bending vibrations of PO_4 groups or the vibration modes of the 4-membered rings of $AlPO_4$ chains. Peak around 450 cm^{-1} can also be attributed to stretching vibrations of the Zn-O bond.[34]

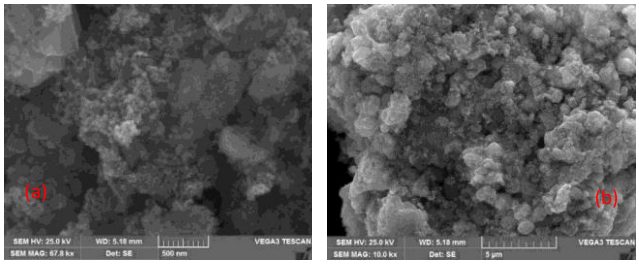

Fig. 3. (a and b) SEM images of ZnO-AlPO composite

Table 1. Elemental Composition of ZnO- AlPO Composite

Element	Weight %	Atomic %
O	35.24	60.70
Al	11.11	11.35
P	11.41	10.15
Zn	42.24	17.81

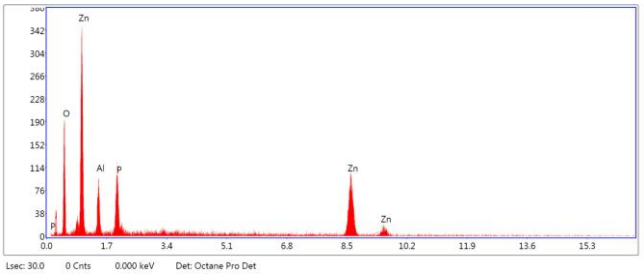

Fig. 4. EDAX plot of ZnO-AlPO composite

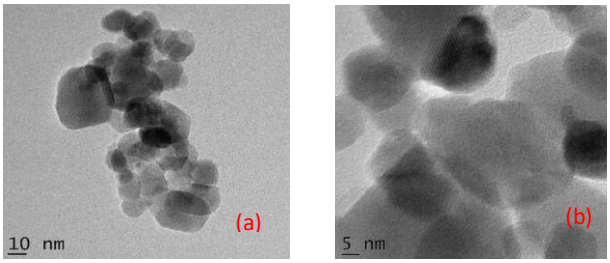

Fig. 5. (a and b) TEM images of ZnO-AlPO composite

3.3. Morphological studies

SEM images of ZnO- AlPO composite are presented in Fig. 3 (a&b). It can be observed that ZnO occupies the pores on the AlPO. The rough surface of ZnO- AlPO along with increased acid sites due to the presence of ZnO makes it a better candidate for adsorption and catalysis when compared to AlPOs. EDAX plot presented in Fig. 4. shows the presence of Zn, Al, P, and O confirming the purity of ZnO-AlPO composite. The percentage composition of elements as determined by EDAX is presented in table 1. TEM images (Fig. 5) show small agglomerated roughly spherical particles with a smooth surface.

3.4. BET analysis of ZnO-AlPO composite

Fig. 6a illustrates Nitrogen adsorption and desorption isotherms of ZnO-AlPO. It exhibits type III hysteresis loop endorsing the presence of aggregates or agglomerates of particles forming slit-shaped pores (plates or edged particles like cubes) with non-uniform size or shapes. A linear plot of [1/W ((P_o/P)-1)] vs P/P_o has been presented in Fig. 6b and the surface area of ZnO-AlPO composite calculated and found to be 21.193 m^2/g. Pore volume and pore diameter of ZnO-AlPO composites were calculated using BJH analysis of nitrogen desorption isotherm and were found to be 0.083 cc/g and 12.83 nm respectively (Fig. 6c) and hence ZnO-AlPO composites can be classified to be microporous in nature.[35]

3.5. TGA-DSC studies

TGA- DSC plot of ZnO-AlPO is presented in fig. 7. It can be observed that there is no loss of molecular mass indicating that there are no

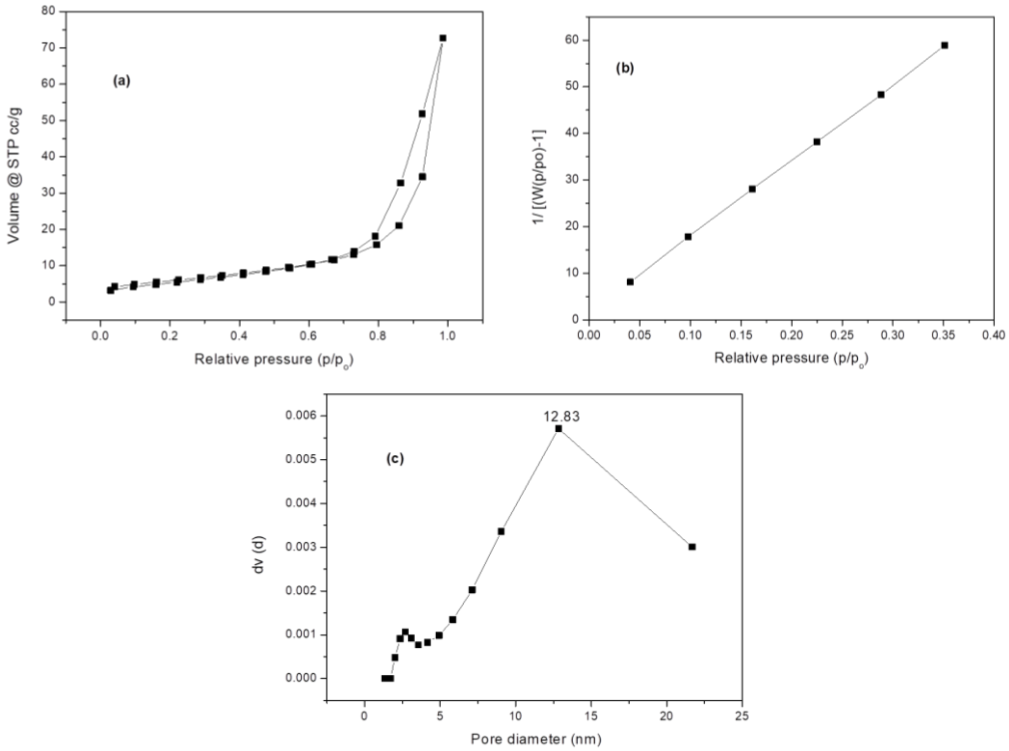

Fig. 6. (a) Nitrogen adsorption-desorption isotherm, (b) multipoint BET plot, and (c) Pore size distribution of ZnO-AlPO composite

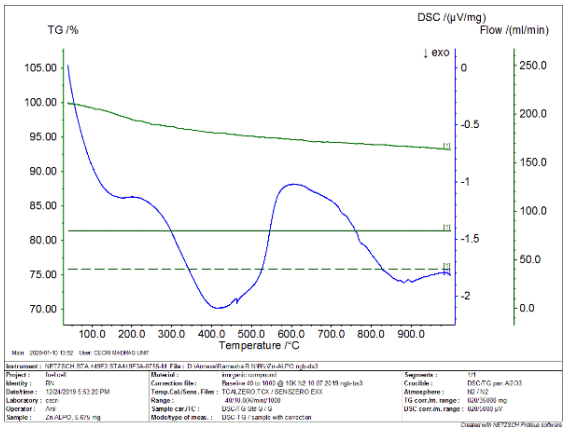

Fig. 7. TGA- DSC plot of ZnO- AlPO composite

organic moieties or water molecules occluded in the system but there is a steady decrease in the molecular mass indicating that thermal stability is slightly low when compared to AlPO tridymite. However, the internal energy of the molecule drops down completely at 500^{O}C and then increases. Internal energy of the molecule fluctuates rapidly but ultimately it reduces to a minimum.[36]

3.6. Adsorption studies

Results of batch sorption studies were analyzed to understand the effect of critical factors such as time, pH, adsorbent dosage, and initial dye concentration of methylene blue adsorbtion on adsorbent. The results were also analyzed using kinetic models and adsorption isotherms to gain an insight into the mechanistic aspects of the process.

3.6.1. Effect of pH

Adsorption of dye is sensitive to the pH of the medium. In the present case, adsorption of methylene blue was found to be maximum at pH 9 (fig. 8).

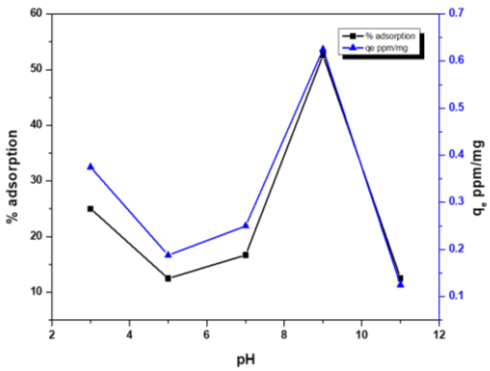

Fig. 8. Effect of pH

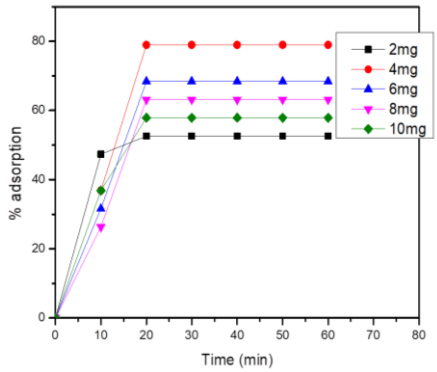

Fig. 9. Effect of adsorbent dosage

Table 2. General parameters calculated for adsorption of Methylene Blue on to ZnO-AlPO

C_o	C_e	q_e	% adsorption
1	0.273	4.545	72.727
2	0.75	7.81	62.5
3	1.174	11.413	60.867
4	1.714	14.285	57.15
5	2.187	17.578	56.26

Where, C_o - Initial concentration in ppm, C_e- equilibrium concentration in ppm, q_e- equilibrium adsorption capacity in ppm

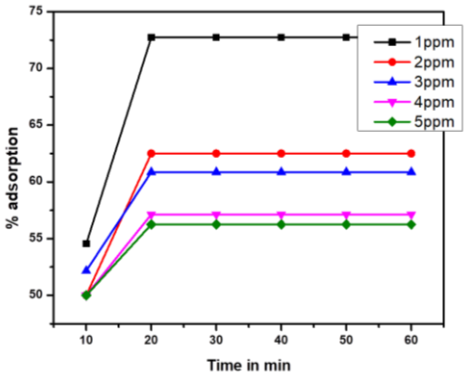

Fig. 10. Effect of initial dye concentration

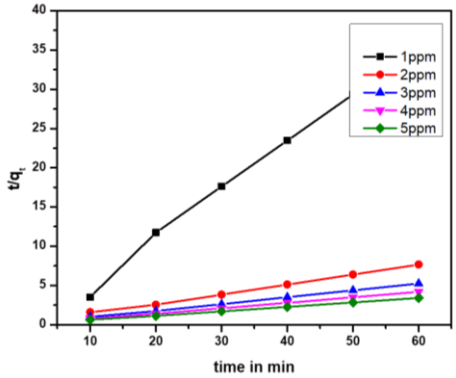

Fig. 11. Pseudo bimolecular mechanism

3.6.2. Effect of dosage

Increase in adsorbent dosage results in increased aggregation of adsorbent molecules that leads to a reduction in the number of adsorption sites. This can be observed in fig. 9, where an increase of dosage from 2 mg to 4 mg shows a sharp increase in the percentage of adsorption while further increase in dosage shows a gradual decrease of adsorption percentage. However, from the graph, it can be observed that irrespective of adsorbent dosage adsorption equilibrium is attained within the initial 20 min.

3.6.3. Effect of initial dye concentration

Results of batch sorption experiments with varying initial dye concentrations are presented in fig. 10. It can be observed that irrespective of the initial dye concentration, adsorption process reaches equilibrium within the initial 20 min. however, the percentage of adsorption decreases with increasing initial dye concentration as active sites get clogged at the earliest with increased initial dye concentration.

Table 3. Kinetic parameters for adsorption of methylene blue on ZnO-AlPO composite

	C_o, ppm	Q_e, ppm	Kinetic Model	Parameters
Pseudo second order Kinetics	1	4.545	0.03249	0.9981
	2	7.810	0.02453	0.9991
	3	11.413	0.02346	0.9996
	4	14.285	0.02119	0.9997
	5	17.578	0.02068	0.9998

Where, Co- initial concentration in ppm, q_e- equilibrium adsorption capacity, K_2- rate constant for pseudo-second-order adsorption, R^2 or r- Pearson correlation coefficient

Table 4. Parameters and r or R^2 values for different adsorption isotherms for MB vs ZnO-AlPO composite

Sl. No	Isotherm	Parameters		R^2
1	Langmuir's Isotherm	b_o	31.45	1
		Q_o	0.5137	
2	Freundlich's isotherm	1/n	0.6491	0.9959
		K_f	10.1718	
3	Temkin's Isotherm	K_T	0.1655	0.9366
		b_T	1.8625	
4	Harkin - Jura Isotherm	A	12.39	0.9915
		B	1.373	
5	Halsey Isotherm	n	0.6491	0.9668
		k	10.17	
6	Redlich-peterson isotherm	β_{bR}	1.434	0.9864
		Kr	1.0073	

3.6.4. Kinetic studies

Results obtained by different batch sorption studies were analyzed to study the kinetic behavior of adsorption of methylene blue on to ZnO-AlPO. General parameters of the adsorption study including the percentage of adsorption are presented in table 2. Data obtained was analyzed using two kinetic models, Lagergren pseudo-first-order kinetic model, and Ho Mc Kay's pseudo-second-order model. It was found that data obtained from adsorption studies of Methylene blue v_s synthesized adsorbents fits better with Ho Mc Kay's pseudo-second kinetic model. A graph of t/qt vs time in minutes is presented in fig. 11 and the kinetic parameters for pseudo-second-order kinetics such as q_e, K_2, and R^2 or r are presented in table 3.

3.6.5. Adsorption isotherms for methylene blue v_s. ZnO-AlPO composite

Adsorption isotherms for methylene blue v_s ZnO-AlPO composite are presented in Fig 12(a-f). All the data corresponding to each adsorption isotherm presented in Table 4 indicate adsorption of methylene Blue on to ZnO- AlPO composite follows Freundlich's adsorption Isotherm (R^2= 0.9959) which is multilayer adsorption with K_f (Freundlich constant of adsorption efficiency) being 10.17 showing adsorption of methylene blue on to ZnO-AlPO is better than other adsorbents studied. R^2 values corresponding to Temkin (0.9366), Harkin Jura (0.9915), Halsey (0.9668), and Redich -Peterson isotherm (0.9864) were found to be between 0.9 and 1 indicating that the process is multilayer adsorption that follows a heterogeneous adsorption mechanism.

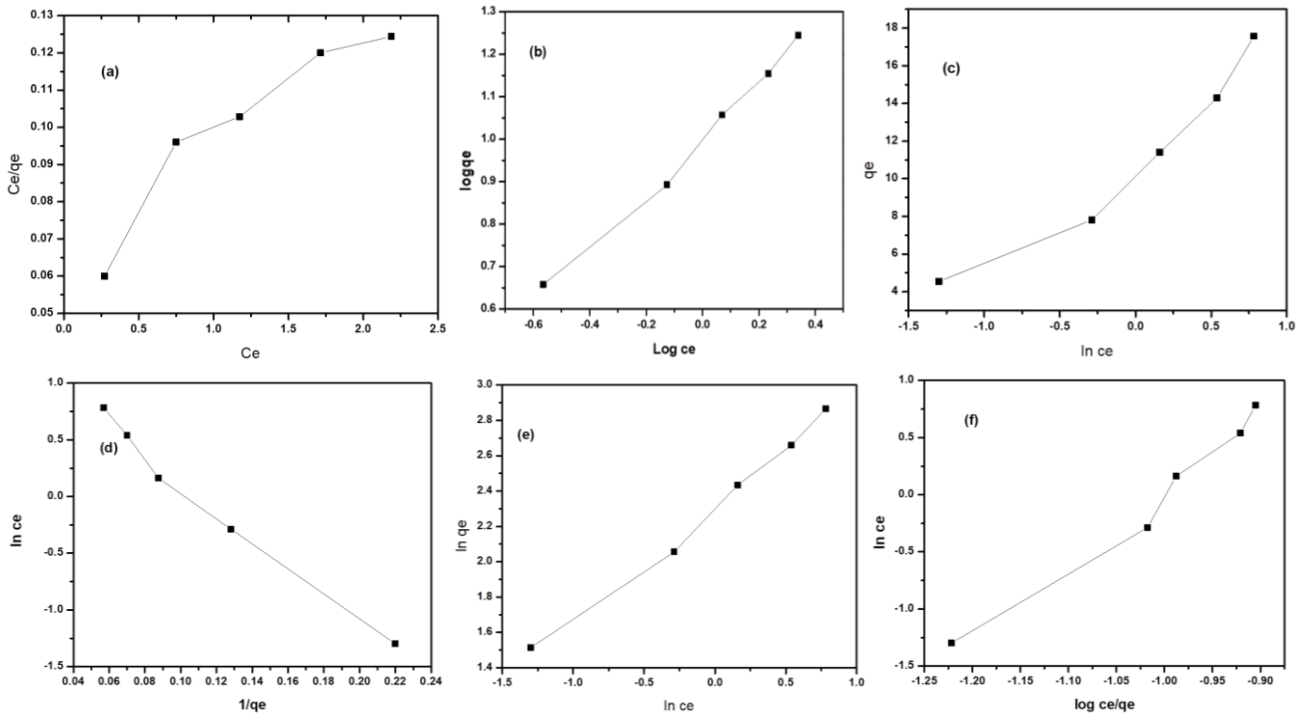

Fig. 12. Adsorption Isotherms for methylene blue v_s ZnO-AlPO composite (a) Langmuir (b) Freundlich (c) Temkin (d) Harkin jura (e) Halsey (f) Redlich Peterson adsorption isotherms.

Table 5. Comparison of surface parameters of AlPO and ZnO-AlPO

Parameters	AlPO	ZnO-AlPO
Surface area (m^2/g)	2.743	21.193
Pore Volume (cm^3/g)	0.004	0.083
Pore diameter (nm)	1.92	12.83
% Adsorption	65	73

Compared to alanine templated aluminophosphate zeolites,[26] post-synthetic modification to synthesize ZnO- AlPO results in a reduction in particle size but it enhances the surface area, pore-volume, and pore diameter. Table 5 presents comparison of the surface parameters of aluminophosphate zeolites and ZnO-AlPO composites.

4. Conclusions

Green synthesis of MO-AlPO composites was found to be facile, environment-friendly, quick, and economical. ZnO-AlPO composite was synthesized with the orthorhombic phase of the AlPO and Hexagonal phase of ZnO. The surface area of the ZnO-AlPO composite was found to be 21.193 m^2/g with a pore volume of 0.083 cm^3/g and a pore diameter of 12.83 nm. SEM and TEM images reveal that ZnO-AlPO composites have a particle size of 10 to 30nm. Particles are well-formed and less agglomerated. TGA- DSC studies show that ZnO-AlPO is more thermally stable. Adsorption of Methylene blue by ZnO-AlPO was found to be a multilayer adsorption that follows Freundlich's adsorption isotherm with an adsorption percentage of 72%. It was observed that the rate of the adsorption process was directly proportional to initial dye concentration. An increase in adsorbent dosage, however, initially increases the rate of adsorption but the later decreases as agglomeration increases decreasing the surface area of adsorption.

Acknowledgements

The authors are grateful to STIC-Cochin for characterization facilities. The authors also thank SIT- Tumkur, University College of Science, Tumkur University, Tumkur, and Maharani's Science College for Women, Bangalore for providing infrastructure facilities for the synthesis of adsorbents and adsorption studies.

Conflicts of Interest

The authors declare no conflict of interest.

References

1 Krishnan S.K.; Singh E.; Singh P.; Meyyappan M.; Nalwa H.S. A Review on Graphene-Based Nanocomposites for Electrochemical and Fluorescent Biosensors. *RSC Adv.*, 2019, **9**, 8778-8881. [CrossRef]
2 Jiang D.; Murugadoss V.; Wang Y.; Lin J.; Ding T.; Wang Z.; Shao Q.; Wang C.; Liu H.; Lu N.; Wei R. Electromagnetic Interference Shielding Polymers And Nanocomposites- A Review. *Polym. Rev.*, 2019, **59**, 280-337. [CrossRef]
3 Zare E.N.; Makvandi P.; Ashtari B.; Rossi F.; Motahari A.; Perale G. Progress in Conductive Polyaniline-Based Nanocomposites For Biomedical Applications: A Review. *J. Med. Chem.*, 2019, **63**, 1-22. [CrossRef]
4 Saleh T.A.; Fadillah G. Recent Trends in the Design of Chemical Sensors Based on Graphene–Metal Oxide Nanocomposites for the Analysis of Toxic Species and Biomolecules. *TrAC Trends in Anal. Chem.*, 2019, **120**, 115660. [CrossRef]
5 Hussain F.; Hojjati M.; Okamoto M.; Gorga R.E. Polymer-Matrix Nanocomposites, Processing, Manufacturing, and Application: An Overview. *J. Compos. Mater.*, 2006, **40**, 1511-1575. [CrossRef]
6 Camargo P.H.C.; Satyanarayana K.G.; Wypych F. Nanocomposites: Synthesis, Structure, Properties and New Application Opportunities. *Mater. Res.*, 2009, **12**, 1-39. [CrossRef]

7 Saraswathi M.S.S.A.; Nagendran A.; Rana D. Tailored Polymer Nanocomposite Membranes Based on Carbon, Metal Oxide and Silicon Nanomaterials: A Review. *J. Mater. Chem. A*, 2019, **7**, 8723-8745. [CrossRef]
8 Prasanna S.S.; Balaji K.; Pandey S.; Rana S. Metal Oxide based Nanomaterials and their Polymer Nanocomposites. *Nanomaterials and Polymer Nanocomposites*. 2019, 123-144. [CrossRef]
9 Dakshayini B.S.; Reddy K.R.; Mishra A.; Shetti N.P.; Malode S.J.; Basu S. Naveen S.; Raghu A.V. Role of Conducting Polymer and Metal Oxide-Based Hybrids for Applications in Ampereometric Sensors and Biosensors. *Microchem. J.*, 2019, **147**, 7-24. [CrossRef]
10 Wilson S.T.; Lok B.M.; Messina C.A.; Cannan T.R.; Flanigen E.M. Aluminophosphate Molecular Sieves: A New Class of Microporous Crystalline Inorganic Solids. *J. Am. Chem. Soc.*, 1982, **104**, 1146-1147. [CrossRef]
11 Milestone N.B.; Tapp N.J. Aluminophosphates as Possible Alternatives to Zeolites. *Stud. Surf. Sci. Catal.*, 1988, **36**, 553-562. [CrossRef]
12 Rajic N.Z. Open-Framework Aluminophosphates: Synthesis, Characterization and Transition Metal Modifications. *J. Serb. Chem. Soc.*, 2005, **70**, 371-391. [CrossRef]
13 Yu J.; Xu R. Insight into the Construction of Open-Framework Aluminophosphates. *Chem. Soc. Rev.*, 2006, **35**, 593-604. [CrossRef]
14 Karanikolos G.N.; Garcia H.; Corma A.; Tsapatsis M. Growth of $AlPO_4$-5 and CoAPO-5 Films from Amorphous Seeds. *Micropor. Mesopor. Mater.*, 2008, **115**, 11-22. [CrossRef]
15 Lakhane M.; Khairnar R.; Mahabole M. Metal Oxide Blended ZSM-5 Nanocomposites as Ethanol Sensors. *Bull. Mater. Sci.*, 2016, **39**, 1483-1492. [CrossRef]
16 Azim M.M.; Stark A. Ionothermal Synthesis and Characterisation of Mn-, Co-, Fe- and Ni- Containing Aluminophosphates. *Micropor. Mesopor. Mater.*, 2018, **272**, 251-259. [CrossRef]
17 Wan B.Z.; Huang K. MnAPO-5 as a Catalyst for Ethane Oxydehydrogenation. *Appl. Catal.*, 1991, **73**, 113-124. [CrossRef]
18 Bae J.W.; Kim S.M.; Kang S.H.; Chary K.V.; Lee Y.J.; Kim H.J.; Jun K.W. Effect of Support and Cobalt Precursors on the Activity of $Co/Alpo_4$ Catalysts in Fischer–Tropsch Synthesis. *J. Mol. Catal. A: Chem.*, 2009, **311**, 7-16. [CrossRef]
19 Bailie J.; Hutchings G.; O'Leary S. "Supported Catalysts," *Encyclopedia of Materials: Science and Technology*. Elsevier, 2001, 8986-8990. [CrossRef]
20 Solís D.; Agudo A.L.; Ramírez J.; Klimova T. Hydrodesulfurization of Hindered Dibenzothiophenes on Bifunctional Nimo Catalysts Supported on Zeolite–Alumina Composites. *Catal. Today*, 2006, **116**, 469-477. [CrossRef]
21 Khan E.A.; Hu E.; Lai Z. Preparation of Metal Oxide/Zeolite Core–Shell Nanostructures. *Micropor. Mesopor. Mater.*, 2009, **118**, 210-217. [CrossRef]
22 Wang F.; Liang L.; Ma J.; Sun J. Synthesis of Fe Substituted Aluminophosphate Feapo-5 Zeolite with Mesoporosity in Compressed CO_2 for the Improved Catalytic Activity. *Mater. Lett.*, 2013, **111**, 201-203. [CrossRef]
23 Leela K.; Devi A. Isolation, Purification and Application of Secondary Metabolites from Lichen *Parmelia Perlata*. *Biosci. Biotech. Res. Asia*, 2017, **14**, 1413-1428. [CrossRef]
24 Kyslychenko O.A.; Protska V.V.; Zhuravel I.O.; Hutsol V.V. The Study of Volatile Compounds of *Parmelia Perlata* Thallus. *Pharmacia*, 2018, **65**, 11-16. [CrossRef]
25 Sharma A.K.; Sharma M.C.; Dobhal M.P. Phytochemical Investigation of Therapeutic Important Lichen: *Parmelia Perlata*. *J. Nat. Prod. Plant Resour.*, 2012, **2**, 101-106. [CrossRef]
26 Shalini K.S.; Nirmala B. Microwave Assisted Green Synthesis, Characterisation of Alanine Templated Aluminophosphate Zeolite and Study of Its Application as Adsorbent. *Appl. Ecol. Environ. Sci.,* 2019, **7**, 231-237. [CrossRef]
27 Banerjee S.; Chattopadhyaya M.C.; Srivastava V.; Sharma Y.C. Adsorption Studies of Methylene Blue onto Activated Saw Dust: Kinetics, Equilibrium, and Thermodynamic Studies. *Environ. Prog. Sustainable Energy*, 2014, **33**, 790-799. [CrossRef]
28 Kannan C.; Muthuraja K.; Devi M.R. Hazardous Dyes Removal from Aqueous Solution over Mesoporous Aluminophosphate with Textural Porosity by Adsorption. *J. Hazard. Mater.*, 2013, **244**, 10-20. [CrossRef]
29 Bharathi K.S.; Ramesh S.T. Removal of Dyes using Agricultural Waste as Low-Cost Adsorbents: A Review. *Appl. Water Sci.*, 2013, **3**, 773-790. [CrossRef]
30 Yagub M.T.; Sen T.K.; Afroze S.; Ang H.M. Dye and its Removal from Aqueous Solution by Adsorption: A Review. *Adv. Colloid Interface Sci.*, 2014, **209**, 172-184. [CrossRef]
31 Monshi A.; Foroughi M.R.; Monshi M.R. Modified Scherrer Equation to Estimate more Accurately Nano-Crystallite Size using XRD. *World J Nano Sci. Eng.*, 2012, **2**, 154-160. [CrossRef]
32 Karthik K.; Dhanuskodi S. Synthesis and Characterization of Zno Nanoparticles by Microwave Assisted Method. *Int. J. Emerg. Technol. Innov. Res*, 2018, **5**, 1022. [CrossRef]
33 Soares V.A.; Xavier M.J.S.; Rodrigues E.S.; de Oliveira C.A.; Farias P.M.A.; Stingl A.; Ferreira N.S.; Silva M.S. Green Synthesis of ZnO Nanoparticles using whey as an Effective Chelating Agent. *Mater. Lett.*, 2020, **259**, 126853. [CrossRef]
34 Akolekar D.B.; Bhargava S.; Van Bronswijk W. Fourier Transform Raman Spectroscopy of Novel Aluminophosphate Molecular Sieves. *Appl. Spectrosc.*, 1999, **53**, 931-937. [CrossRef]
35 Zeng Y.; Phadungbut P.; Do D.D.; Nicholson D. Anatomy of Adsorption in Open-End and Closed-End Slit Mesopores: Adsorption, Desorption, and Equilibrium Branches of Hysteresis Loop. *J. Phys. Chem. C*, 2014, **118**, 25496-25504. [CrossRef]
36 Zholobenko V.; Garforth A.; Dwyer J. TGA-DTA Study on Calcination of Zeolitic Catalysts. *Thermochim. Acta*, 1997, **294**, 39-44. [CrossRef]